Type of paper: full-length article (Journal Name –**Powder technology**)
Date text written: 09/2019
Data text revised: 10/2019
Number of words in the main text = 7103
Number of figures = 22
Number of tables = 3

Network analysis of heat transfer in sphere packings

Author 1
Wenbin Fei, PhD student
Department of Infrastructure Engineering, The University of Melbourne, Parkville, Australia
ORCID: 0000-0002-9275-8403

Author 2
Guillermo A. Narsilio✉, PhD, MSc (Math), MSc (CE), CEng
Department of Infrastructure Engineering, The University of Melbourne, Parkville, Australia
ORCID: 0000-0003-1219-5661

Author 3
Joost H. van der Linden, PhD.
Department of Infrastructure Engineering, The University of Melbourne, Parkville, Australia

Author 4
Mahdi M. Disfani, PhD, MSc, BSc
Department of Infrastructure Engineering, The University of Melbourne, Parkville, Australia
ORCID: 0000-0002-9231-8598

Full contact details of the corresponding author
Guillermo A. Narsilio, Associate Professor
Engineering Block B 208, Department of Infrastructure Engineering, The University of Melbourne, Parkville, VIC 3010, Australia
Email: narsilio@unimelb.edu.au, Phone: +61 (3) 8344 4659, Fax: +61 (3) 8344 4616

Abstract

Porosity-dependent models can be used to predict the effective thermal conductivity (ETC) of particulate materials. However, they cannot directly account for microstructural features such as particle connectivity and interparticle contact area. Complex network theory can be used to extract network features as microstructural characteristics. However, these features have not been used to study heat transfer. In this work, both contact network and thermal networks are constructed for mono-disperse and poly-disperse sphere packings. Network features are extracted using complex network theory and machine learning techniques are applied to investigate the correlation between these features and the ETC. The most relevant thermal and contact network features for predicting thermal conductivity are identified. The network features capturing both interparticle connectivity and contact quality, such as "weighted degree", show high correlation with ETC. Furthermore, random forest regression results show that involving multi-network features in a model enhance the accuracy in predicting ETC.

Keywords: Complex network theory; Graph theory; Heat transfer; Machine learning, Microstructure.

1 Introduction

Heat transfer in geomaterials is a dominant process in the design and construction of various engineering applications including geothermal engineering [1], petroleum engineering [2], carbon dioxide geology storage [3] and radioactive waste disposal [4]. The thermal conductivity λ is a key parameter used to describe and quantify heat transfer processes commonly encountered in many of the above applications. Hence, understanding and being able to accurately estimate the effective thermal conductivity (ETC) of geomaterials are of great importance.

Models [5-13] used to predict the ETC of static granular materials can be roughly classified into two types: mixing-law models and packing structure models. *Mixing-law models* combine the thermal conductivity of the different phases found in the materials based on solid volume fraction or porosity to estimate an overall ETC. Examples of models related to the volume fractions of the solid are series models [14], parallel models [14] and geometric mean models [15]. Porosity-dependent models are summarised by Abdulagatova et al. [11]. However, solid volume fraction and porosity are characteristics at the sample scale, leading mixing-law models to potentially neglecting the effect of microstructure [5, 16-19]. Most of these models can be used only within certain limited ranges of porosity. They are rarely valid for the entire (wide) porosity range encountered in materials, especially for materials with large solid-fluid thermal conductivity ratio ($\lambda_s/\lambda_f \to \infty$) [11]. For instance, Maxwell's model [20] is proposed to predict the ETC of randomly distributed and non-interacting spheres packings with large porosity. Modifications are required, though, for the model to be valid for medium porosity [21] and low porosity materials [22].

As an alternative, *packing structure models* are employed to predict ETC by replacing porosity with certain structural characteristics. A better understanding of the microstructure in granular materials can also assist in designing artificial (granular) materials [23-25]. Batchelor and O'Brien [26] found that heat flux was related to the minimum gap between particles and the mean of the particles' local curvature. Finney [27] introduced a method to measure particle connectivity using Voronoi tessellation and Cheng et al. [28] proposed two models based on the connectivity of particles. These models are valid in a wide range of solid-fluid thermal conductivity ratios. However, these works were performed based on mono-sized sphere packings. Later, Siu and Lee [29] investigated dry simple cubic (SC), body-centered cubic (BCC) and face-centered cubic (FCC) packings and found that the ETC of a disperse sphere packing bed was related to one of these structures and had a linear relationship with contact radius ratio (the ratio of contact radius to particle radius) under the chosen structure. However, to use these models for other granular materials, one must first match their porosity and microstructure to the closest of SC, BCC or FCC and estimate the contact radius ratio of these materials before using the proposed relationship. Therefore, parameters are required to characterise the microstructure of granular materials and their correlations with ETC need to be investigated.

Complex network theory is available to characterise the microstructure and connectivity based on the network built according to the topology of a material [30, 31]. A network is a collection of nodes that are linked by edges. Different networks can be constructed and the meanings of nodes and edges change along with the type of the network. For example, in a pore network, a node is created to represent a pore and an edge represents a pore throat connecting them [32]. In a contact network, each node indicates a particle and an edge connects two nodes when two particles are in contact [31]. Newman [33] reviewed the theory, development and applications of complex network theory. Tools arising from complex network theory have the advantage of capturing succinct, inherent multi-scale properties to present the structure, topology, dynamics and functionality of the network [34].

In geotechnical engineering, complex network theory has been applied to investigate the behaviours of granular materials such as mechanical stability and fluid flow. Russell et al. [35] proved that contact networks and pore networks contained important information about the jamming-unjamming dynamics and preferential paths in a deforming granular material, respectively. van der Linden et al. [31] quantified the connectivity of the pores and particles using a pore network and a particle contact network, respectively, and then applied machine learning techniques to study their correlations to fluid flow. The network features extracted from a contact network may be correlated well to heat transfer because heat conducts primarily through the contact area between particles. However, heat also conducts through small gaps [13] between particles and this gap is not considered in a classical contact network. A *thermal* network that considers these small gaps or 'near contacts' was built [36, 37] to compute the ETC of sphere packings. Although contact networks and thermal networks have been built for spherical granular materials, complex network theory has not been employed to extract microstructure and connectivity features and to characterise heat transfer in granular materials.

This work aims to identify the most relevant network features for predicting ETC in dry granular materials. Firstly, mono-disperse and poly-disperse sphere packings are generated using a discrete element method (DEM) and networks representing these packings are derived. Then the network features and ETC of each packing are computed with complex network theory and the finite element method, respectively. Network features are computed both for the contact network and the thermal network. Machine learning techniques are then employed to investigate the correlation of network features with the ETC. Next, the importance of individual network features to the ETC for mono-disperse and poly-disperse packings are analysed. The general performance of network features on all samples is also investigated.

2 Methods

A framework that integrates several techniques is proposed to identify the most relevant physical variables and (new) network features affecting heat transfer in granular materials using complex network theory (Fig. 1). In step 1, DEM is used to generate synthetic mono-disperse and poly-disperse

sphere packings. These various packings are used both to compute the ETC via the finite element method in step 2 and to construct networks and extract network features using complex network theory in step 3. Then, the calculated features are collected in step 4 and used in several machine learning algorithms to select the 'best fit' model for each feature in step 5. Finally, the importance of the features is analysed and compared in step 6. The details of each component in this framework are discussed in the following subsections.

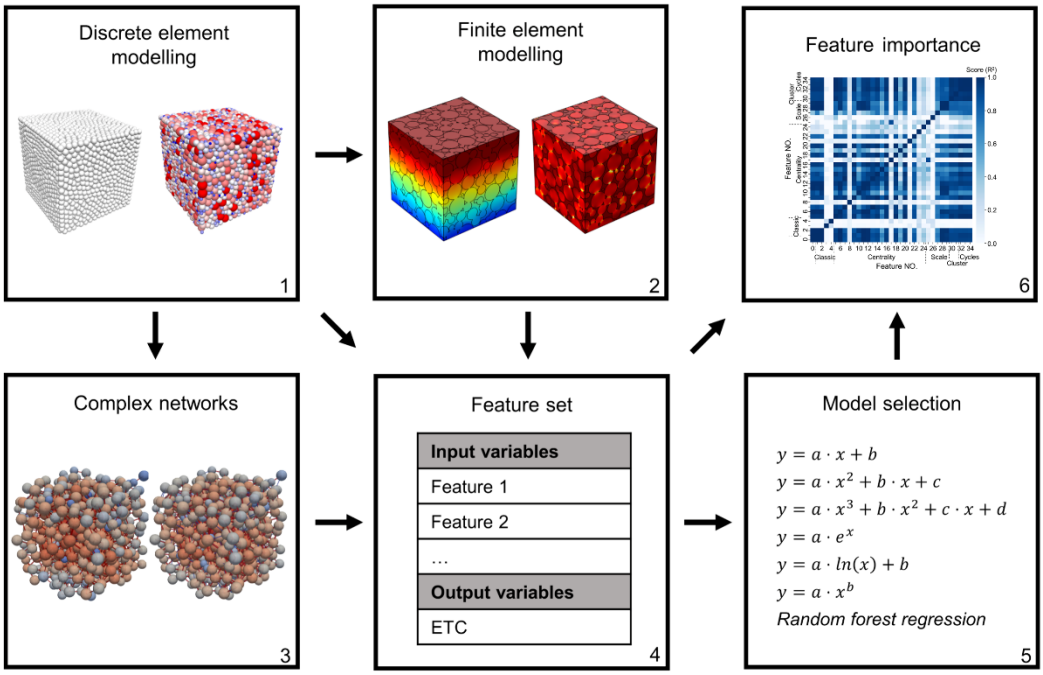

Fig. 1 Mono-disperse and poly-disperse sphere packings are generated in step 1. Heat transfer is simulated using the finite element method to calculate the effective thermal conductivity (ETC) in step 2. In step 3, a contact network and a thermal network are constructed for each packing; then complex network theory is used to extract network features. In step 4, classic physical parameters, network features and ETC are collected. Machine learning techniques are used to select the proper model for each feature to find its correlation coefficient with ETC in step 5. Finally, the relative importance of each feature is computed and compared.

2.1 Discrete element modelling

Numerical mono-disperse and poly-disperse assemblies are constructed using the PFC software [38]. Spheres are assembled in a cubic box with dimensions of $10 \times 10 \times 10\ mm$. Twenty-four mono-disperse and twenty-four poly-disperse packings are generated using the parameters shown in Table 1. The porosity in PFC can be used as an input parameter to generate each assembly. The friction coefficient is selected as zero in this work to enhance the particle rearrangement. Spheres in dense mono-disperse packings may overlap to simulate changing interparticle contact area [36, 39] which is

important in heat transfer. Representative element volume (REV) subsamples with dimensions of $4.55 \times 4.55 \times 4.55\ mm$ are sampled from the centre of the assemblies. The selected REV size results in a REV/D_{50} ratio of 7.6×7.6×7.6 which is larger than 5.8×5.8×3 as previously suggested in paper [39] and 7.1×7.1×3.6 used in paper [40]. The total number of particles in our model (~280) is almost three times the value recommended by Kanit et al (2003) [41]. Examples of the assemblies of mono-disperse and poly-disperse packings are shown in Fig. 2.

Table 1 Simulation parameters used in PFC

Grain shape	Spherical
Density [kg/m^3]	2550
Local damp coefficient	0.7
Friction coefficient	0
Grain radius [mm]	0.3 for mono-disperse packings 0.1-0.5 for poly-disperse packings
Porosity	0.14-0.35

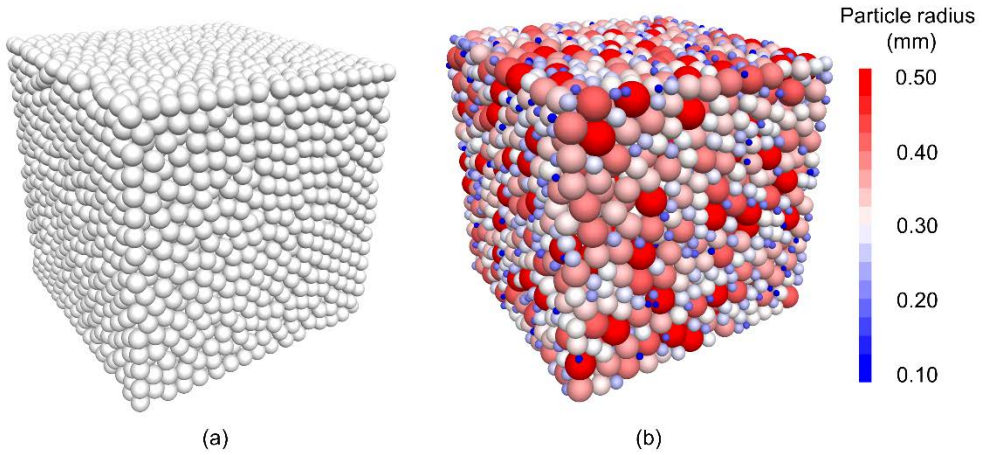

Fig. 2 Sphere packings are generated in PFC (a) mono-disperse packing, (b) poly-disperse packing. Both of the two packings have the porosity of 0.28.

2.2 Finite element simulation

The geometry of each sample constructed with PFC is imported into Simpleware ScanIP [42] to generate finite element meshes. A mesh size sensitivity analysis was conducted in previous related works by the authors [43, 44] to ensure that the computed ETC convergences to an asymptotic value. In this work, the mesh comprises 9,516,529 tetahedral elements as shown in Fig. 3 (a). The number of the elements across the particle (average) diameter is approximately 28. The selection of D_{50}/(mesh size) ≈28 larger than that in simulating fluid flow in heterogeneous sandstone (D_{50}/(mesh size) ≈ 10 as suggested in paper [45] and 17.6 as suggested in paper [46]) and in simulating heat transfer (D_{50}/(mesh size) ≈ 17 in paper [39]. As a result, the mesh size selected here is considered small enough for

computing a reasonable accurate thermal conductivity. Once created, the finite element meshes are transferred to COMSOL Multiphysics [47] to simulate heat transfer by solving [48] :

$$\rho C \frac{\partial T}{\partial t} + \rho C u \cdot \nabla T = \nabla \cdot (\lambda \nabla T) + Q \quad (1)$$

where, for each phase involved in the simulation (solid grains, air or water in the pore space), ρ is the density [kg/m^3], C is the heat capacity [J/(kg K)], T is the temperature [K], t is the time [s], u is the velocity vector [m/s], λ is the thermal conductivity [W/(m K)]. The thermal conductivity of the solid phase is taken as 3 W/(m K) [13, 36, 49] and the air thermal conductivity, as 0.025 W/(m K) in this work, Q is the heat sources [W/m^3], nil in all cases analysed here, but included for completeness.

The conductive heat flux vector q can be computed using the simplest form of Fourier's law:

$$q = \lambda \nabla T \quad (2)$$

Additionally, to ensure the continuity at the particle-pore interface, a continuity equation is used to compensate the system [39]:

$$-n(q_s - q_p) = 0 \quad (3)$$

where n is the unit normal vector of the solid-pore interface, q_s and q_p are the heat fluxes in the particle and pore, respectively.

All samples are simulated using the same heat transfer model and boundary conditions. An example of the mesh and simulation results are shown in Fig. 3. The boundary temperature on the top is 293 K while the temperature on the bottom is 292 K, to generate a small temperature gradient along the vertical axis. Other boundaries are set as insulated. Given the heat fluxes at inlet and outlet planes, the ETC on these two boundaries can be computed using [39]:

$$\lambda_{eff} = \frac{\frac{1}{A}\int_A Q_z \, dA}{\frac{T_a - T_b}{L}} \quad (4)$$

where λ_{eff} is the ETC of a sample [W/(m K)], A is the horizontal cross-section area of the sample [m^2], T_a = 293 K and T_b = 294 K at the inlet and outlet boundary temperatures, L is the height of the sample [m], Qz is the vertical heat flux of nodes at the inlet or outlet [W/m^2].

Finally, the average value of the two thermal conductivities at the inlet and outlet is taken as the ETC of the whole sample.

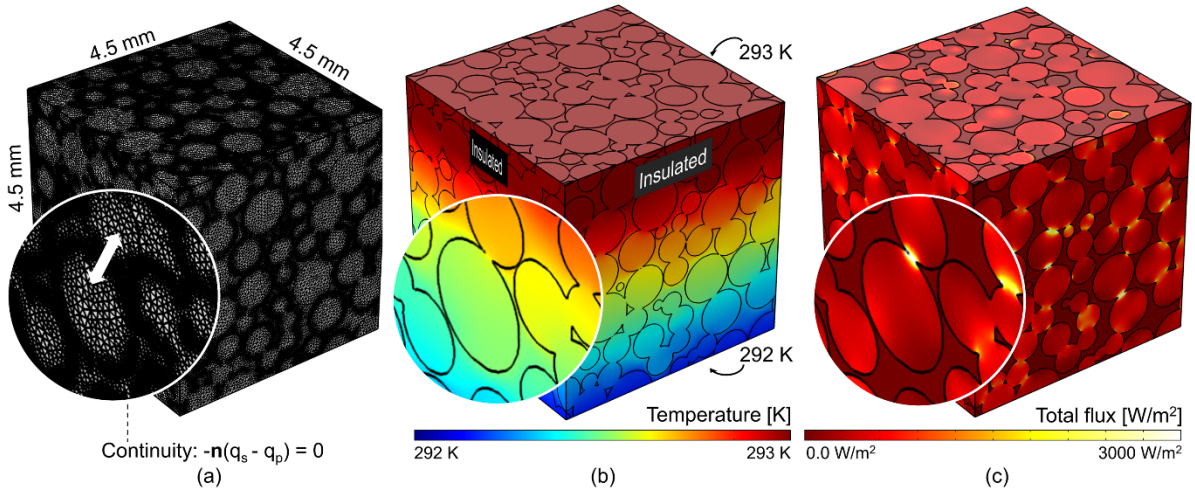

Fig. 3 Finite element mesh and heat transfer simulation results (a) mesh generated from Simpleware ScanIP, (b) temperature distribution, and (c) heat flux distribution.

2.3 Complex network features

A *contact* network is built by allocating a node at each particle centroid and an edge is created when particles are in contact (shown at the bottom of Fig. 4). In dry granular materials, heat travels not only within particles (path 1 in Fig. 4) and through the interparticle contact area (path 2 in Fig. 4) but also via particle-fluid-particle conduction (path 3 in Fig. 4), particle-particle radiation (path 4 in Fig. 4) and pore fluid convection (path 5 in Fig. 4). As radiation becomes important after the temperature is above 1000 K and convection mode is relevant when D_{50} is larger than 6mm [13, 50], heat transfer is mostly attributed to conduction [13, 51] in dry granular materials. Therefore, a *thermal* network is established by assigning nodes to particle centroids and allocating edges to both the real contacts (schematically in red in Fig. 4) and near-contacts (schematically in blue in Fig. 4), similar to what is proposed in paper [36].

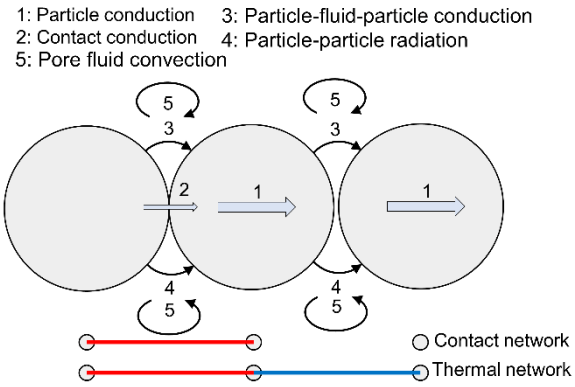

Fig. 4 Heat conducts through not only the physical contact(s) between particles (path 2) but also through the pore space (paths 3, 4 and 5). Hence, an edge is also assigned to the near-contact in a thermal network.

Once the networks are built, complex network theory is employed to extract multiscale network features. The network features can be categorised into four types: (1) Centrality, (2) Network scale, (3) Cycle and (4) Clustering.

2.3.1 Centrality

Centrality indicates the node position and the "significance" of a node in the network, with varying types of centrality defining this significance in distinct ways. Five metrics for measuring centrality are calculated in this paper: *degree, closeness centrality, node betweenness centrality, edge betweenness centrality and eigenvector centrality*. The *degree* $\kappa(i)$ of a node is measured as the number of edges linked to a node. The *degree* calculated from the contact network is the well-known *coordination number*.

Closeness centrality is a measure of the distance of a node to all others. A node with high *closeness centrality* $[G^*]_C$ indicates it is at a 'central' position. If using V to indicate the set of vertices in networks, the *closeness centrality of node* $i \in V$ can be computed as [52]:

$$[G^*]_C(i) = \beta \left[\sum_{j=1}^{|V|-1} d(i,j) \right]^{-1} \tag{5}$$

where *d(i,j)* is the shortest path between node $i, j \in V$ and β is a normalisation term. β is set as the number of reachable nodes $(|V|-1)$ and as the number of max possible edges $[|V|(|V|-1)]/2$ in this work, respectively.

Betweenness centrality characterises the importance of a node or an edge as the bridge between other nodes or edges in a network. A node with high *node betweenness centrality* or an edge with high *edge betweenness centrality* means that it is important for heat to transfer through. *Betweenness centrality* $[G^*]_B$ of a node or an edge is computed as [53]:

$$[G^*]_{B^{node}}(i) = \beta \sum_{j,k \in V} \frac{\sigma(j,k|i)}{\sigma(j,k)} \tag{6}$$

where $\sigma(j,k)$ is the total number of shortest paths from node *j* to *k*, $\sigma(j,k|i)$ is the number of shortest paths from node *j* to *k* and overpass *i*. Similarly, the *edge betweenness centrality* can be calculated by computing $\sigma(j,k|e)$ as the number of shortest paths from node *j* to *k* that overpass edge e. β is a normalisation term, equal to $2/[|V-1|(|V|-2)]$ for *node betweenness centrality* and $2/[|V|(|V|-1)]$ for *edge betweenness centrality*.

Eigenvector centrality considers the contribution of nodes to the connectivity of the whole network and indicates the node which has wide-reaching influence in a network. Relative scores are assigned to

all nodes in a network and the score is high if a node is highly connected to other nodes who also have high score [54].

Fig. 5 illustrates the difference between different centrality features in the same network. A node has a high degree but may have low eigenvector centrality if edges hold similar low score. In a social network, a node with high betweenness centrality also may have low eigenvector centrality if it is away from the power centres in the network.

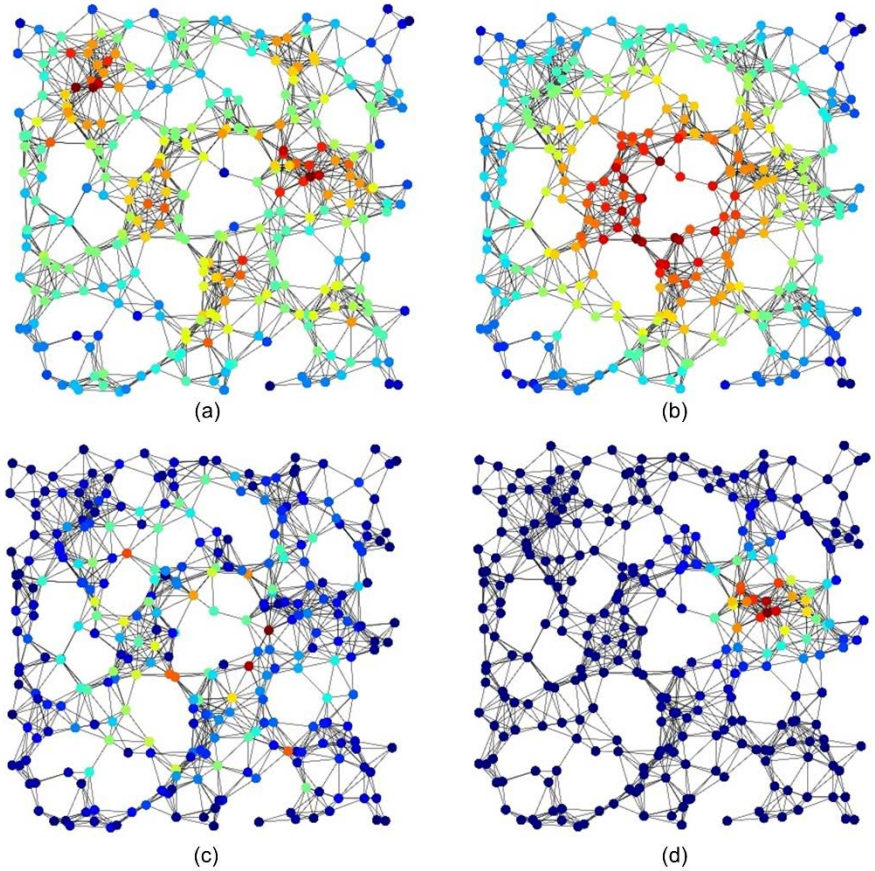

Fig. 5 Example of the same contact network and its different centrality values for nodes: (a) Degree, (b) Closeness centrality, (c) Betweenness centrality and (d) Eigenvector centrality. Each definition of centrality highlights different significances of centrality at nodes. The colour shows the value of each feature, red means high value while blue represents low value.

2.3.2 Network scale

Network scale is a measure indicating the average distance of one node from another in a network. This information is used to interpret how rapidly something can spread through a network. Network diameter and average shortest path length can be used to present the network scale. More nodes are reachable in a network with a smaller network diameter and smaller average shortest path length. The two different networks in Fig. 6have the same number of nodes. However, from node 1 to the bottom of the network, four other nodes are reachable in two steps in the ring network (a) while six other nodes

can be reached in two steps in the tree network (b). Furthermore, it takes two steps to reach the end in the tree network, while three steps are required to reach the end (node 7) in a ring network. In other words, a process (e.g. heat transfer) propagates faster in the tree network (b) than in the ring network (a). Network scale can be quantified by *Network diameter* G_D^*, *average shortest path length* $[G^*]_{P_w}$ and *network density* G_ρ^*. *Network diameter* G_D^* is the longest one of the shortest paths between two nodes in the network and it can be normalised by |V|-1 to be $[G^*]_{P_w}$. In this work, we also introduce the *average shortest path length between nodes at inlet and outlet* $[G^*]_{P_w^{tp}}$ because it resembles a heat transfer path. Moreover, we employ *network density* G_ρ^*, which describes the ratio of the actual edge number to the potential edge number in a network,

$$G_\rho^* = \frac{|E|}{|V| \cdot (|V| - 1)} \tag{7}$$

where E is the set of edges in a network.

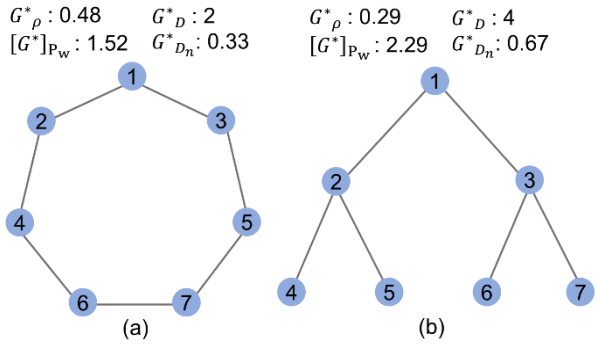

Fig. 6 Network diameter and average shortest path length can indicate the network structure: (a) a ring type network and (b) and tree like network with the same number of nodes shown as examples.

2.3.3 Cycles

A cycle in a network is a loop of edges that starts and ends at the same node. An *l-cycle* is a cycle containing *l* edges. By assuming straight edges between nodes, a *3-cycle* is a triangle. Cycles in granular materials help describe the mesoscale structure of networks [55-58] which make them appealing since mesoscale features are vital to the behaviour of granular systems [59]. For instance, a triangle is an inherently rigid structure, so the number of *3-cycle* in contact network can hint the rigidity of granular materials [44, 60].

2.3.4 Clustering

Clustering implies how integrated or fractured the overall network system is. *Clustering coefficients* are calculated as the *degree* of local clusters. Global clustering coefficient G_{GC}^* [34] measures the density of the triangles in a network using Eq. 8 while the local clustering coefficient $[G^*]_{LC}$ in Eq. 9 [61] quantifies the fraction of triangles through each node [44]:

$$G^*_{GC} = 3\,\frac{number\ of\ triangles}{number\ of\ connected\ triples} \tag{8}$$

where a triple means that three nodes can generate either three edges or two edges.

$$[G^*]_{LC}\,(\mathrm{i}) = \frac{2T(i)}{\kappa(i)[\kappa(i)-1]} \tag{9}$$

where *T(i)* is the number of triangles (or *3-cycles*) through node *i*, and κ(i) is the degree of node *i*.

A network with a high *clustering coefficient* indicates the presence of more local clusters, i.e. the network is more fractured (Fig. 7).

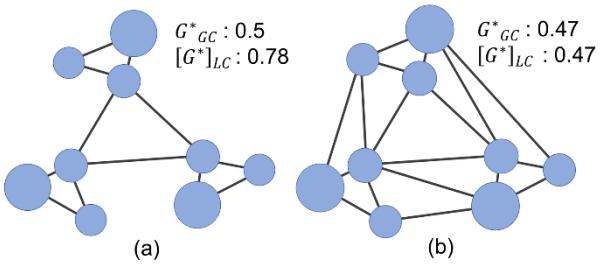

Fig. 7 Clustering features example: an integrated network (a) shows lower clustering coefficients than a fractured network (b).

2.4 Feature set

For each sample, the network features described in section 2.3 are computed for each contact network and thermal network. As higher contact area and thermal conductance are related to larger heat transfer fluxes, and higher *degree* indicates more interparticle contacts, the *degree* is weighted by interparticle contact area in the contact network and thermal conductance in the thermal network. In other words, the weighted degree $\kappa_w(i)$ of each node $\mathrm{i} \in V$ is $\kappa(i)$ multiplied by contact area and thermal conductance. In contrast, most of the other network features are computed based on the shortest path which is calculated with the minimisation of edge weighting. Hence, edge length for calculating these network features is weighted by the reciprocal of the contact area in the contact network and the reciprocal of thermal conductance in the thermal network.

If the weighted network features have dimensions (m^2 from a weighted contact network and W/K from a weighted thermal network), the features in the contact network will be normalised by D_{50}^2 in the contact network and normalised by $(\lambda_{solid} \cdot D_{50})$ in the thermal network to make all the features dimensionless. In addition to the network features, classic physical parameters including porosity, contact radius ratio (the ratio of the radius of contact area to the radius of the neighbouring particle), coefficient of uniformity and coefficient of curvature are calculated. All the features are summarised in Table 2.

Table 2 Feature notation.

Type	NO.	Notation	Attribute
Classic	1	n	Porosity
	2	γ	Contact radius ratio
	3	C_u	Coefficient of uniformity
	4	C_c	Coefficient of curvature
Centrality	5	$[G^*]_\kappa$	Degree
	6	$[G^*]_{\kappa_w}$	Weighted Degree
	7	$[\mathrm{G}^*]_\mathrm{C}$	Closeness centrality
	8	$[\mathrm{G}^*]_{\mathrm{C_{n1}}}$	Closeness centrality normalised by $\lvert V\rvert - 1$
	9	$[G^*]_{C_{n2}}$	Closeness centrality normalised by $[\lvert V\rvert(\lvert V\rvert - 1)]/2$
	10	$[G^*]_{C_w}$	Weighted closeness centrality
	11	$[G^*]_{C_{nw1}}$	Weighted closeness centrality normalised by $\lvert V\rvert - 1$
	12	$[G^*]_{C_{nw2}}$	Weighted closeness centrality normalised by $[\lvert V\rvert(\lvert V\rvert - 1)]/2$
	13	$[G^*]_{B^{node}}$	Node betweenness centrality
	14	$[G^*]_{B_n^{node}}$	Normalised node betweenness centrality
	15	$[G^*]_{B_w^{node}}$	Weighted node betweenness centrality
	16	$[G^*]_{B_{nw}^{node}}$	Normalised weighted node betweenness centrality
	17	$[G^*]_{B^{edge}}$	Edge betweenness centrality
	18	$[G^*]_{B_n^{edge}}$	Normalised edge betweenness centrality
	19	$[G^*]_{B_w^{edge}}$	Weighted edge betweenness centrality
	20	$[G^*]_{B_{nw}^{edge}}$	Normalised weighted edge betweenness centrality
	21	$[G^*]_{B_w^{edge^{tp}}}$	Weighted top-to-bottom edge betweenness centrality average
	22	$[G^*]_{B_{nw}^{edge^{tp}}}$	Normalised weighted top-to-bottom edge betweenness centrality average
	23	$[G^*]_E$	Eigenvector centrality
	24	$[G^*]_{E_w}$	Weighted eigenvector centrality
Network scale	25	G_ρ^*	Network density
	26	G_D^*	Network diameter
	27	$G_{D_n}^*$	Normalised network diameter
	28	$[G^*]_{P_w}$	Weighted shortest path (average)
	29	$[G^*]_{P_w^{tp}}$	Weighted shortest path from between nodes at inlet and outlet (average)
Clustering	30	$G^*{}_{GC}$	Global clustering coefficient
	31	$[G^*]_{LC}$	Local clustering coefficient
Cycles	32	G_{3C}^*	The number of 3-cycle3-cycle
	33	$[G^*]_{3C^{node}}$	Average number of node 3-cycleAverage node 3-cycle
	34	$[G^*]_{3C^{\mathrm{edge}}}$	Average number of edge 3-cycle Average edge 3-cycle

Note that $[G^*]$ is a unified indicator of a network feature, specifically, $[G^C]$ [55] means a feature is calculated from the contact network while $[G^T]$ means a feature is based on the thermal network. The brackets in $[G^*]$ are used to denote the average value of a parameter. Degree $[G^C]_\kappa$ computed from the contact network is equivalent to the well-known classic coordination number.

As the range of values of different features varies widely, in order to weigh them equally, feature scaling is employed by subtracting the average and dividing by the standard deviation (Equation 10):

$$\widetilde{x_i} = \frac{x_i - \mu(X)}{\sigma(X)} \tag{10}$$

where X = (x_1, x_2, …, x_n) is one of the features from Table 2, μ is the average and σ is the standard deviation of the feature X.

2.5 Model selection

As a broad feature set is shown in Table 2, we aim to identify the most 'important' features in each group for predicting the ETC. To compute the importance, supervised machine learning techniques are employed to fit a model, predict the performance of the model and calculate the score of each feature. Six models are tested (linear, quadratic polynomial, cubic polynomial, exponential, logarithmic, power), generically listed in Equations 11-16, to fit the relationship between individual features (typically x) and the ETC (typically y). In order to apply the models more efficiently, nonlinear models are transformed into a linear format.

$$y = ax + b \tag{11}$$

$$y = aX_1 + bX_2 + c, \quad X_1 = x^2, \quad X_2 = x \tag{12}$$

$$y = aX_1 + bX_2 + cX_3 + d, \quad X_1 = x^3, \quad X_2 = x^2, \quad X_3 = x \tag{13}$$

$$Y = A + bx, \quad Y = ln(y), \quad A = ln(a) \tag{14}$$

$$y = aX + b, \quad X = ln(x) \tag{15}$$

$$Y = bX + A, \quad Y = ln(y), \quad A = ln(a) \tag{16}$$

Then lasso regression [62], a modified linear regression for avoiding overfitting, is used to train models and calculate the correlation between individual features and ETC. For each feature, six models are trained and the one rendering the highest correlation is selected as the 'best fit' model. Additionally, random forest regression [52] is employed to study the effect of multi-feature (or multi-variable) correlations on ETC.

2.5.1 Regressions

1. Lasso regression

Linear regression is simple and effective. However, quadratic polynomial and cubic polynomial models are prone to overfit the training data set. One available method of mitigating the overfitting in polynomial models is to implement regularisation. The regularisation is applied by penalising the errors between trained and predicted values. Lasso regression [62] is one of the regularisation methods embedded in the python library scikit-learn [63] and has been employed in this work.

2. Random forest regression

A random forest [64, 65] constructs multiple decision trees at training time and merges the output of the individual trees to obtain a more accurate prediction. Here, a decision tree [66] is a predictive model based on a branching series of Boolean tests. A merit of the random forest algorithm is that the relative importance of each feature can be easily measured.

2.5.2 Cross-validation

Scarce data used in machine learning may lead to insufficient data for the test set, which then may result in a poor estimation of the generalisation performance. A widely used method to mitigate this issue is K-fold cross-validation [67]. K-fold cross-validation is a resampling procedure and it contains the following steps:

1. Shuffle the data randomly.
2. Split data into K parts.
3. Use K-1 parts as a training set to fit models and the remaining part as a validation set to calculate a score (refer to section 2.6). The procedure has to repeat K times and each model will achieve K scores. The average scores of these models are compared, and then the model with the highest score is selected as the 'best fit' model.

Utilising this approach enables each data point to be used in the validation set once and in the training set K-1 times. In the present work, K is set to 4, which means eighteen samples are used to train models and six samples are used to validate the models in either mono-disperse or poly-disperse samples.

2.6 Feature importance

After selecting the 'best fit' model for each feature, the whole set of data is used as a test set to calculate the generalised performance score of the model. The score of the models under lasso regression is the coefficient of determination R^2. As each feature is adopted in lasso regression models, R^2 also indicates the correlation between the feature and the ETC. Furthermore, R^2 is used to evaluate the performance of random forest regression model. Meanwhile, the importance of each feature in a random forest regression is measured by Gini impurity [68].

3 Results and discussion

The ETC calculated by using finite element method is validated in Section 3.1. Then the importance of individual network features to ETC in mono-disperse and poly-disperse packings are investigated in Section 3.2 followed by a wider generalisation regarding the relevance of network features to ETC in all the samples in Section 3.3.

3.1 Effective thermal conductivity

The ETC computed from finite element modelling and normalised by the thermal conductivity of the solid phase of the packing is shown in Fig. 8 against the porosity *n* of each packing. Our results show good agreement with theoretical results [29], experimental results [69, 70] and modelling results [71] available in the literature. According to Fig. 8, ETC decreases linearly with porosity for both mono-disperse packings and poly-disperse packings. However, the ETC in the two types of samples diverges with the increment of porosity, which indicates that porosity-dependent models may not be sufficient

to cover a wide range of porosity, although it may be sufficiently accurate for particular engineering applications.

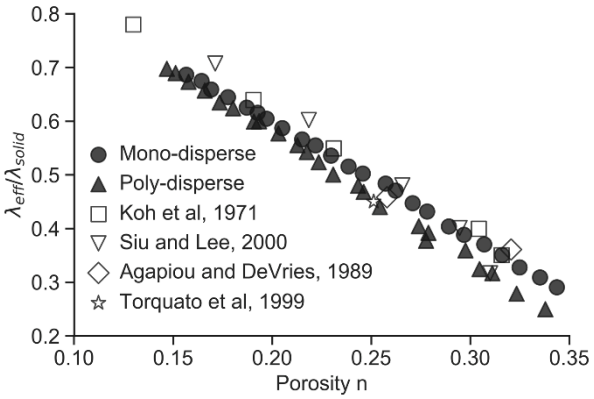

Fig. 8 Computed ETC for mono-disperse and poly-disperse packings in this work (solid symbols) show good agreement with those found in the literature (hollow symbols).

3.2 Importance of network features to ETC in mono-disperse and poly-disperse packings

Both contact network and thermal network are constructed for each packing. The identification of interparticle contacts and near-contacts as well as the calculation of contact area and thermal conductance follow the strategies in paper [36]. The topologies of the networks for the poly-disperse sample with porosity 0.246 is visualised in ParaView [72] as an example (Fig. 9). In Fig. 9, the contact network (a) show fewer edges than the thermal network (b), 1803 (shown in red) and 2471 (in red and blue), respectively. In other words, 668 near-contacts, shown as blue edges are considered in the thermal network. This difference in the networks may lead to highlight the different heat transfers mechanics within the packings. Network features arising from these networks can capture these differences and these will be explained in more detail in this section.

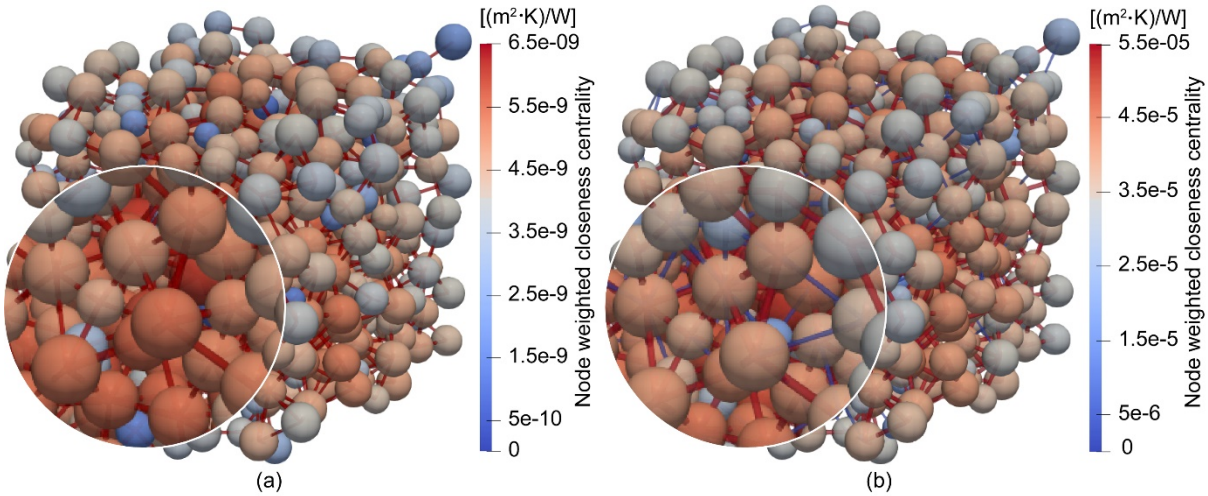

Fig. 9 Networks of the poly-disperse sample with porosity 0.246: (a) Contact network, (b) Thermal network. The colour at nodes represents the node weighted closeness centrality while the colour at edges represents the type of edge (red edges represent particle contacts while the blue edges represent near-contacts). The node size is scaled by particle radius.

3.2.1 Importance of contact networks features

In this section, the importance of each feature in Table 2 to ETC is assessed using its score and consistency. The score R^2, ranging from 0 to 1, is computed between each feature and the ETC by applying six models with lasso regression (Section 2.5.1). Furthermore, a feature has a good consistency if its score in mono-disperse and poly-disperse packings are similar.

Fig. 10 depicts the performance of each contact feature on predicting ETC. The various models (Section 2.5) used to calculate the scores are summarised in Appendix 1. It can be observed that 25 out of 34 features have scores larger than 0.8 in mono-disperse while 27 features in poly-disperse packings, which indicates they have good correlations with ETC and the scores are consistent. These features except $G_{D_n}^c$ (Feature 27) render higher scores in mono-disperse packings than in poly-disperse packings. Classic features such as porosity (Feature 1), contact radius ratio (Feature 2) and coordination number (Feature 5) have scores close to 1, as expected.

As shown in Table 2, centrality-type features include degree (Feature 6), closeness centrality (Features 7-12), betweenness centrality (Features 13-22) and eigenvector centrality (Features 23-24). Fig. 10 shows that weighted degree $[G^c]_{\kappa_w}$ (Feature 6) has a high score and consistency than coordination number (Feature 5), which means considering the interparticle contact area in the coordination number (as the weighted degree does) can enhance its correlation to ETC. All the closeness centrality features except $[G^c]_{C_{n1}}$ (Feature 8) in mono-disperse packings have scores higher than 0.85. In particular, $[G^c]_{C_{n2}}$ (Feature 9) and $[G^c]_{C_{nw2}}$ (Feature 12) have both high scores and consistence. Betweenness centrality features also have high scores except for $[G^c]_{B_w^{node}}$ (Feature 15), $[G^c]_{B^{edge}}$ (Feature 17) and $[G^c]_{B_w^{edge}}$ (Feature 19) in both mono-disperse and poly-disperse packings. However, when normalised, these three features show high scores (Features 16, 18 and 20) and good consistency. In contrast, eigenvector centrality features do not show good performance, only $[G^c]_{E_w}$ (Feature 24) in mono-disperse packings have a score around 0.93.

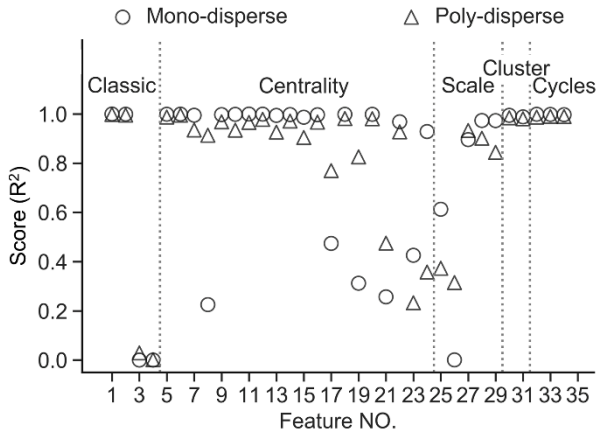

Fig. 10 Scores between contact network features and ETC (feature numbers corresponds to those in Table 2)

Since $[G^c]_\kappa$ (Feature 5) $[G^c]_{\kappa_w}$, (Feature 6), $[G^c]_{C_{nw2}}$ (Feature 12) and $[G^c]_{B_n^{edge}}$ (Feature 18) perform well in both scores and consistency, the original data and fitted models are superimposed in Fig. 11. For a given ETC, mono-disperse packings require more particle contacts (Fig. 11 (a)) and show lower betweenness centrality (Fig. 11 (d)) than poly-disperse packings. It is also shown that $[G^c]_{\kappa_w}$ and $[G^c]_{C_{nw2}}$ tend to collapse the data arising from the two types of packings into just one group. While degree $[G^c]_\kappa$ (or 'classic' condonation number) only considers the particles' connectivity, the weighted degree $[G^c]_{\kappa_w}$ also considers the contact quality (contact area) besides connectivity. As heat conduction depends on the thermal conductivity of solid particles [13], the structure of particle packings [73, 74] and the interparticle contact conductance [13, 75-79] in dry granular packings, $[G^c]_{\kappa_w}$ shows a better performance in predicting ETC than the degree $[G^c]_\kappa$.

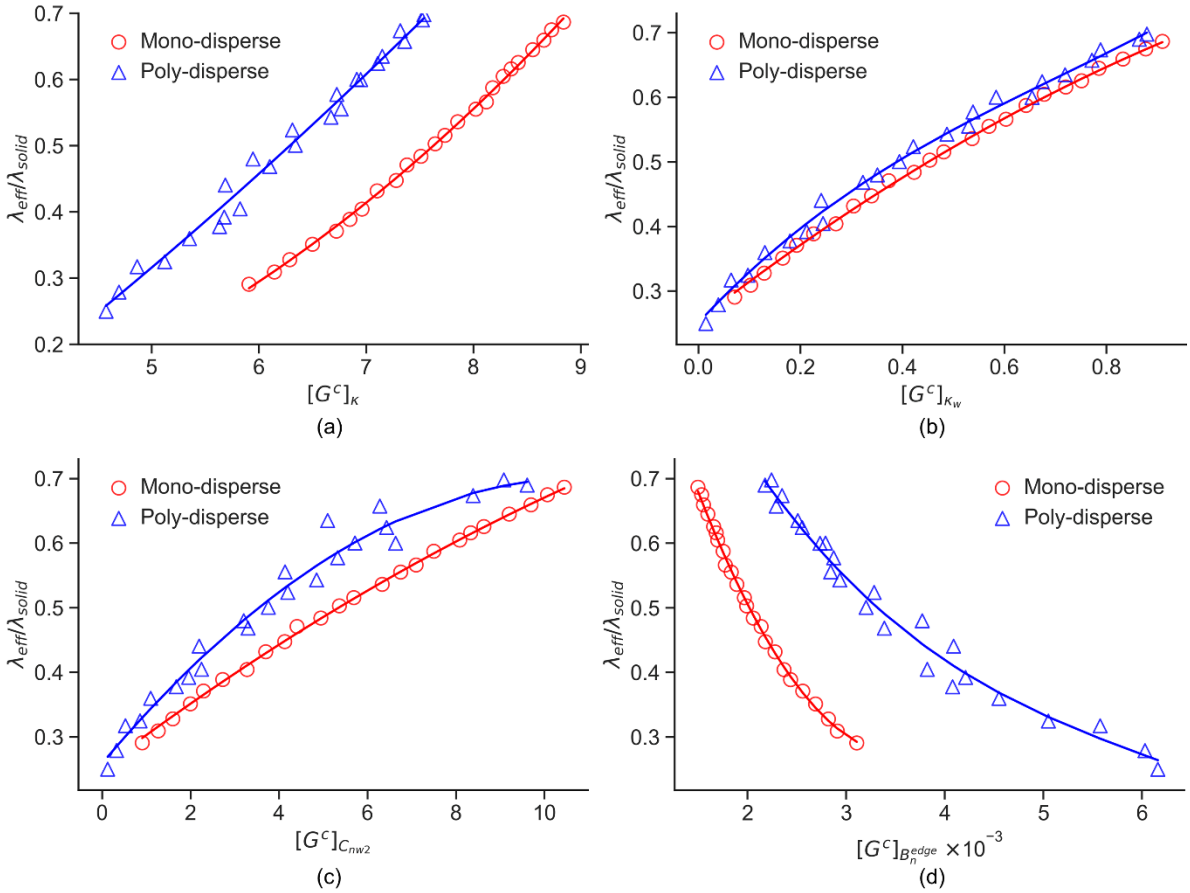

Fig. 11 The relationship between ETC and contact network centrality features: (a) Degree (= coordination number), (b) Weighted degree, (c) Weighted closeness centrality normalised by $[|V|(|V|-1)]/2$, and (d) Normalised edge betweenness centrality. Points in the figure represent the data used to train models while lines represent the predicted values from selected models.

In terms of the scale-type features, average weighted shortest path $[G^c]_{Pw}$ (Feature 28) has a score around 0.97 in mono-disperse packings but around 0.90 in poly-disperse packings. Normalised network diameter $G^c_{D_n}$ (Feature 27) has a lower score than $[G^c]_{Pw}$ in mono-disperse packings but has a better consistency. Fig. 12 shows that ETC decreases with the increase of $[G^c]_{Pw}$ even though $[G^c]_{Pw}$ has a jump when $[G^c]_{Pw}$ is larger than 5×10^{15}. As $[G^c]_{Pw}$ is related to the average contact area of a sphere packing, it can quantify the interparticle contact quality which affects ETC. It also shows a similar score to contact radius ratio γ (Feature 2) when predicting the ETC of mono-disperse packings in Fig. 10. However, it achieves a lower score than γ when applying to predict the ETC of poly-disperse packings because γ considers both the contact area and particle size.

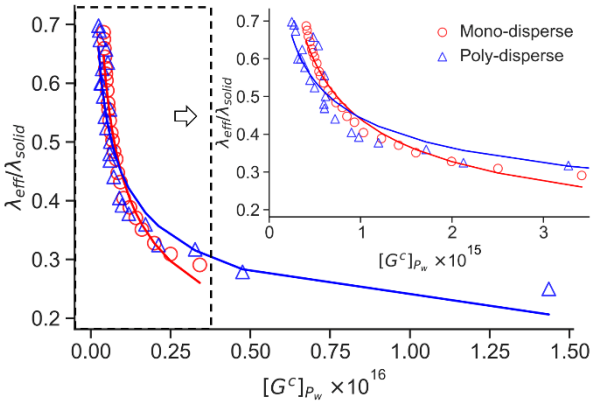

Fig. 12 ETC decreases when increasing the average weighted shortest path. Points in the figure represent the data used to train models while lines represent the predicted values from selected models.

According to Fig. 10, the scores and consistency of cluster-type features and cycle-type features remain high for both mono-disperse and poly-disperse packings. Their relative importance to heat transfer is similar to that of porosity (Feature 1), contact radius ratio (Feature 2) and coordination number (Feature 5), so they can be taken as alternatives to these classical variables or features for predicting the ETC of sphere packings. Fig. 10 also shows that cluster-type features and cycle-type features are better candidates used to predict ETC than scale-type features, which indicates that particle-connectivity is more critical to heat transfer than contact quality in sphere packings.

One feature from each cluster-type features and cycle-type features are selected to show the relationship with ETC in Fig. 13. It can be seen from Fig. 13 (a) that the relationship between the local clustering coefficient (a scale-type feature) and the ETC in mono-disperse has a similar incremental ratio to that in poly-disperse packings. In contrast, Fig (b) shows that the trend between 3-cycle and ETC in mono-disperse are different from that in poly-disperse packings. Hence, the local clustering coefficient is more consistent than 3-cycle for predicting ETC in different types of sphere packings.

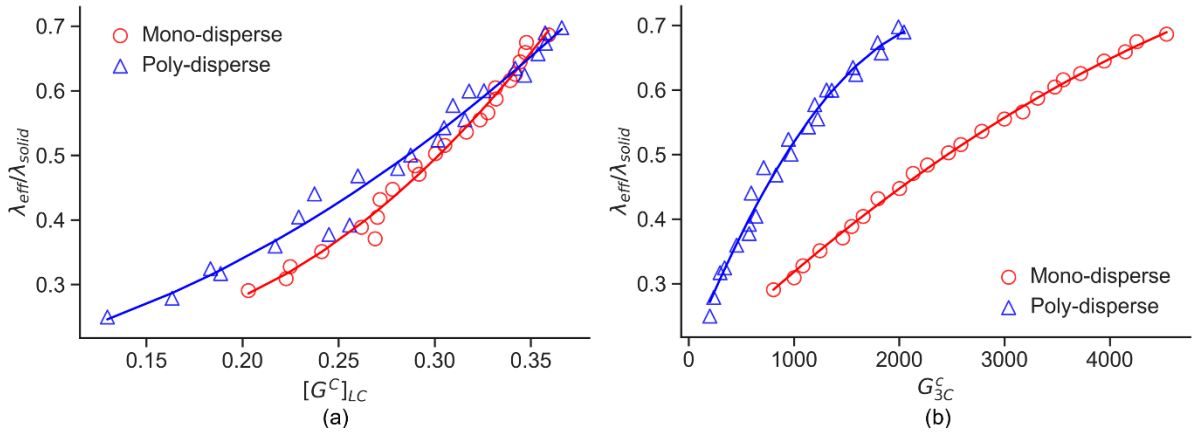

Fig. 13 The relationship between ETC and (a) Global clustering coefficient and (b) 3-cycle. Points in the figure represent the data used to train models while lines represent the predicted values from selected models.

In general, cluster features and cycles features computed from contact networks are shown to be highly relevant for predicting ETC, while scale features are less desirable for such correlations. In addition, all centrality features but eigenvector centrality could be used to predict ETC. In particular, the centrality features such as $[G^c]_{\kappa_w}$ and $[G^c]_{C_{nw2}}$ considering both particle connectivity and contact area are proven to be good candidates to predict ETC.

3.2.2 Importance of thermal network features

Similar to the performance of contact network features, thermal network features whose score are higher than 0.8 also perform better in mono-disperse packings than in poly-disperse packings (Fig. 14 and Appendix 2).

As for the relevance of centrality features computed from thermal networks, weighted degree $[G^T]_{\kappa w}$ (Feature 6), $[G^T]_{C_{nw1}}$ (Feature 11) and $[G^T]_{C_{nw2}}$ (Feature 12) could be the most suitable centrality features for predictability of ETC because they consider both particle connectivity and contact quality. Compared with the vital contact network centrality features in Fig. 10, Fig. 14 shows that less important thermal network centrality features are available in predicting ETC but the available thermal network features have a higher correlation with ETC in both mono-disperse and poly-disperse packings. As the thermal network is an extension of contact network by adding near-contacts as edges, network features considering heat transfer through gaps between neighbouring particles enhance the accuracy of predicting ETC. The original data of the same features in Fig. 11 together with the fitted models are presented in Fig. 15. For each feature, the data are still clustered into two groups corresponding to mono-disperse packings and poly-disperse packings. The correlation for each feature has a similar trend in different groups. However, by comparing Fig. 11 and Fig. 15, it can be observed that the difference of a feature calculated from the thermal network between two types of packings is larger than that from the contact network when aiming to achieve the same ETC. Thermal networks are different from contact networks because they consider near-contacts as edges. As degree measure the edge number, it can be known that more near contacts are required in a mono-disperse packing than in a poly-disperse packing to achieve the same ETC. Weighted degree $[G^c]_{\kappa_w}$ in the contact network measure the contact area at each interparticle contacts, so it indicates the heat transfer through interparticle contacts. In contrast, $[G^T]_{\kappa_w}$ in thermal network measure thermal conductance at both interparticle contacts and near-contacts, it implies the heat transfer through both interparticle contacts and the small gap between neighbouring particles. As the same amount of heat transfer through interparticle contacts in a mono-disperse packing as that in a poly-disperse pacing can achieve the same ETC (Fig. 11 (a)), it indicates

that the heat transfer in dry sphere packings is mainly attributed to the heat transfer through interparticle contacts and the contribution of near-contact to the heat transfer in dry sphere packings is minor. Additionally, more edges in the thermal network reduce the role of the nodes/edges as unique 'bridges'. Hence, the betweenness centrality becomes smaller, resulting in that the fitted two lines in Fig. 15 (d) are further away from each other compared with the distance in Fig. 11 (d)).

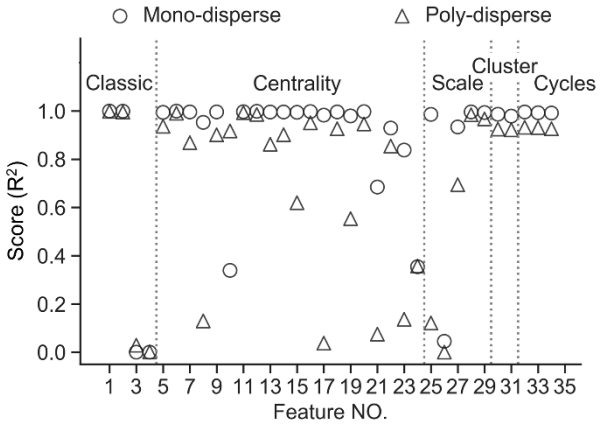

Fig. 14 Scores between thermal network features and ETC (feature numbers are corresponding to Table 2)

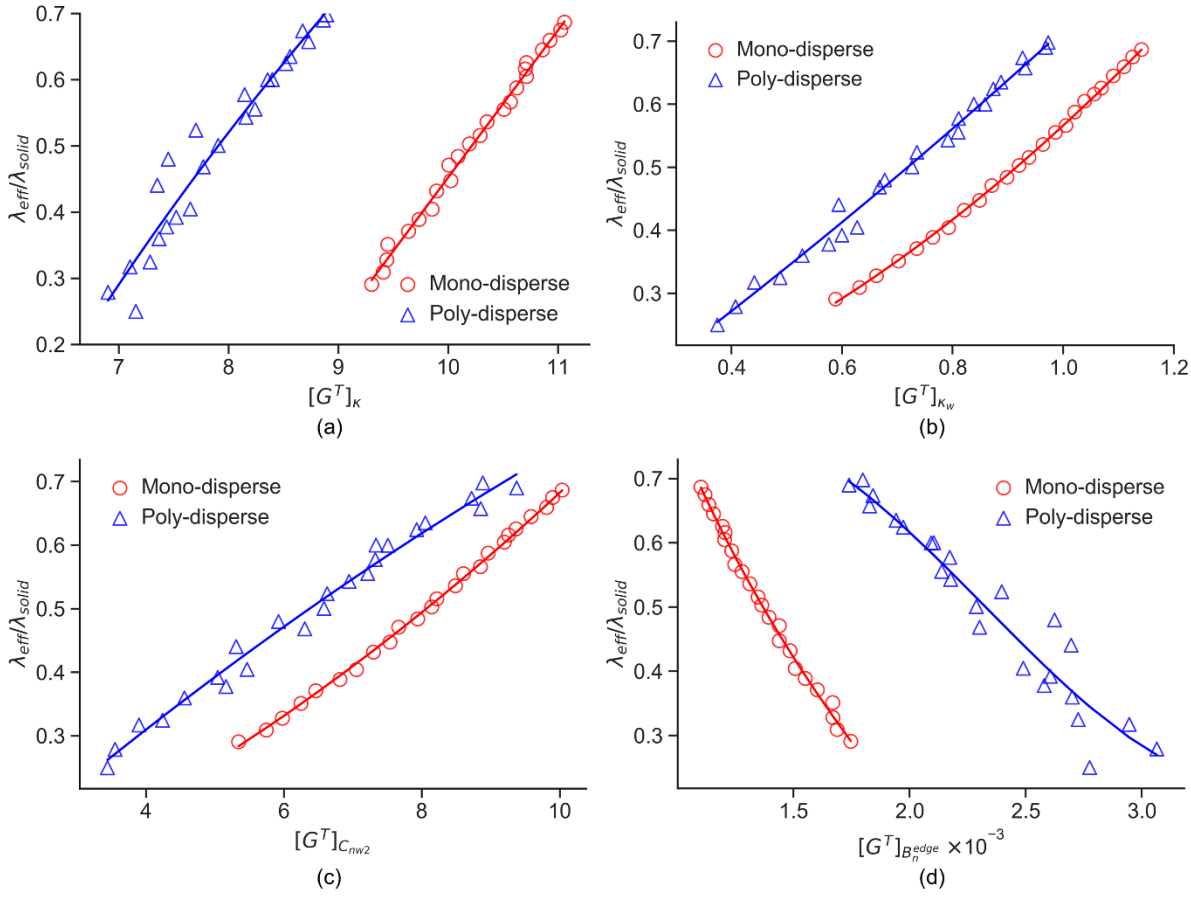

Fig. 15 The relationship between ETC and thermal network centrality features: (a) Degree, (b) Weighted degree, (c) Weighted closeness centrality normalised by $[|V|(|V|-1)]/2$, and (d) Normalised edge betweenness centrality. Points in the figure represent the data used to train models while lines represent the predicted values from selected models.

As for scale features, both $[G^T]_{Pw}$ (Feature 28) and $[G^T]_{P_w^{tp}}$ (Feature 29) are important and relevant given their high scores and consistency. Compared with the trend of the relationship between $[G^C]_{P_w}$ and ETC in Fig. 12, the ETC decreases smoothly with increasing $[G^T]_{Pw}$ (Fig. 16) which considers the heat transfers through near-contacts. Batchelor and O'Brien [26] reported that heat fluxes in particulate materials are influenced by the near-contacts between particles and the mean of the local curvature of neighbouring particles. Indeed, a thermal network also considers the near-contacts as edges, and $[G^T]_{Pw}$ includes thermal conductance through both interparticle contacts and near-contacts in its definition, it is then not surprising that it results in being a highly important feature for predicting the ETC of sphere packings. The different slope of the fitted lines for mono-disperse packings and poly-disperse packings is because the local curvature of neighbouring particles is not involved at each edge.

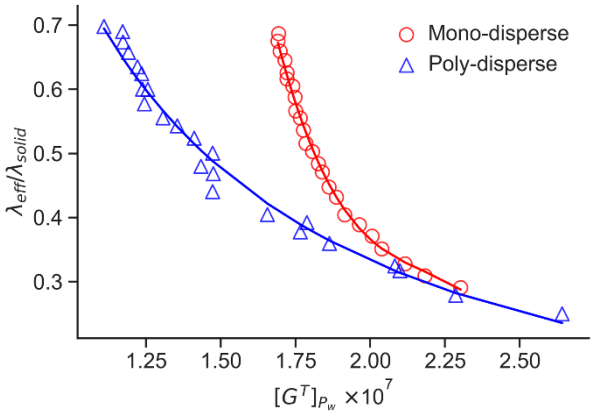

Fig. 16 ETC monotonically and smoothly decreases with the increasing average weighted shortest path GTPw calculated from a thermal network.

All cluster features and cycle features have scores higher than 0.92. To achieve the same ETC, the difference of the local clustering coefficient between mono-disperse packings and poly-disperse packing becomes small with the increase of local clustering coefficient in Fig. 17 (a). In contrast, the value of 3-cycles in poly-disperse packings are always lower than mono-disperse packings as shown in Fig. 17 (b).

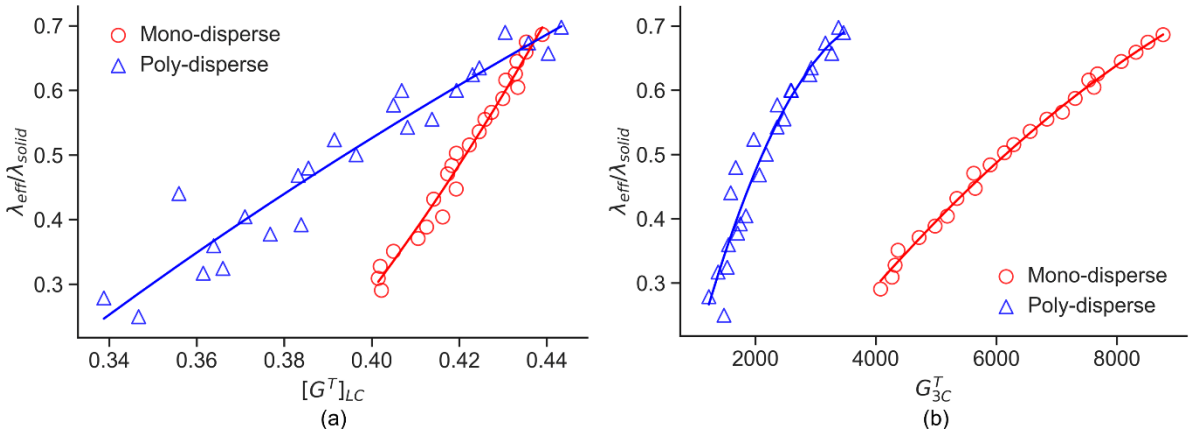

Fig. 17 The relationship between ETC and (a) Global clustering coefficient and (b) 3-cycle. Points in the figure represent the data used to train models while lines represent the predicted values from selected models.

From Fig. 10 and Fig. 14, it is known that many network features show good correlation with ETC, which may be because a strong relationship exists between different network features. Hence, the same model selection and feature importance evaluation methods used to access the scores of the relationship between features and ETC are now applied to investigate the relationships between different network features. The score of correlation between each different pair of thermal features in poly-disperse packings is shown in a heatmap (Fig. 18). It can be seen from Fig. 18 that more than one-third of the score is larger than 0.8. Since $[G^T]_{C_{nw1}}$ (Feature 11), $[G^T]_P$ (Feature 28), $[G^T]_{LC}$ (Feature 31) and G^T_{3C} (Feature 32) are important in each type of thermal network features, the scores of their relationship are high as shown in Table 3 for four types of network features (centrality, scale, clustering, cycles). As these essential features have close interplay relevance and have high scores when predicting ETC (Fig. 14), each of them could be used as an alternative to coordination number or porosity in an equation to predict ETC.

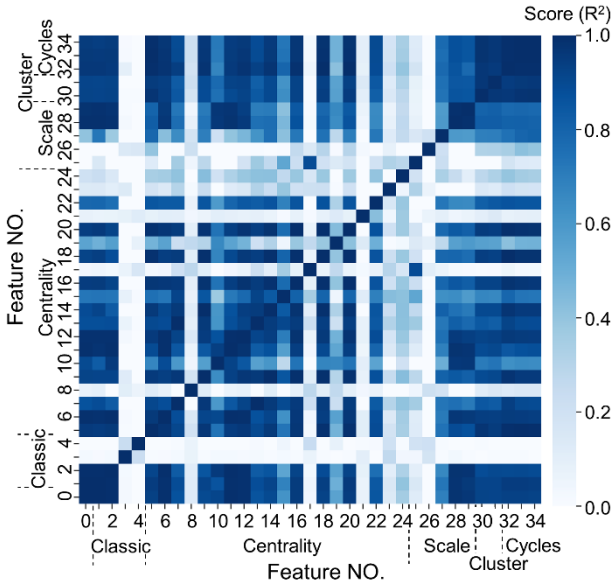

Fig. 18 A heatmap shows the score of correlation between a different pair of features in poly-disperse packings. Feature 0 is the ETC and other feature numbers refer to Table 2.

Table 3 The score of correlation between thermal network features.

	$[G^T]_{C_{nw1}}$ (Feature 11)	$[G^T]_P$ (Feature 28)	$[G^T]_{LC}$ (Feature 31)	G^T_{3C} (Feature 32)
$[G^T]_{C_{nw1}}$ (Feature 11)	1	0.9839	0.9295	0.9564
$[G^T]_P$ (Feature 28)	0.9839	1	0.8509	0.8622
$[G^T]_{LC}$ (Feature 31)	0.9295	0.8509	1	0.9654
G^T_{3C} (Feature 32)	0.9564	0.8622	0.9654	1

Overall, among different types of thermal network features, centrality features including weighted degree and closeness centrality features are essential to heat transfer. Scale features are also available to predict ETC. However, cluster and cycles features perform slightly worse compared with their peers from contact networks.

3.3 Importance of network features to ETC in combined mono-disperse and poly-disperse packings

In section 3.2, we discussed the importance of network features in mono-disperse and poly-disperse packings, respectively. In this section, we investigate the general performance of network features on combined data including both mono-disperse and poly-disperse packings, as one may think of mono-disperse being a sub-set of poly-disperse beds.

Firstly, the correlations of individual features against ETC are computed (Fig. 19). Some contact network features such as $[G^c]_{\kappa_w}$ (Feature 6), $[G^c]_{C_{nw1}}$ (Feature 11) and $[G^c]_{LC}$ (Feature 31) still show high scores (>0.9) while all of the thermal network features show lower scores (<0.8). The relationship

between $[G^c]_{\kappa_w}$ and ETC is fitted into a quadratic polynomial equation (Equation 17) with R^2 of 0.99 as shown in Fig. 20. The high R^2 indicates the correlation between $[G^c]_{\kappa_w}$ and ETC is better than that between porosity (Feature 1) and ETC, which also can be observed by comparing Fig. 20 and Fig. 8. The contact network features having high scores means the data from mono-disperse packings are closer to the data from poly-disperse packings as shown in Fig. 11(b), Fig. 11(c) and Fig. 13 (a). In contrast, the low score of contact network features and thermal network features in combined packings is the result of the clustering of the data into two groups corresponding to mono-disperse packings and poly-disperse packings as shown from Fig. 11 to Fig. 13 and Fig. 15 to Fig. 17. Furthermore, clustering of the data still manifests for the difference of the same network features from thermal networks and contact networks. The reason is that near-contacts are considered in the thermal network but they seem to contribute little to heat transfer in dry spheres as explained in section 3.2.2. However, the contribution of near-contacts may become important in wet sphere packings [43] or when considering radiation [80] between particles, important only at high temperatures. In order to investigate the potential applicability of thermal network features in more complex conditions, we attempt to analyse the correlation between multiple-features and ETC.

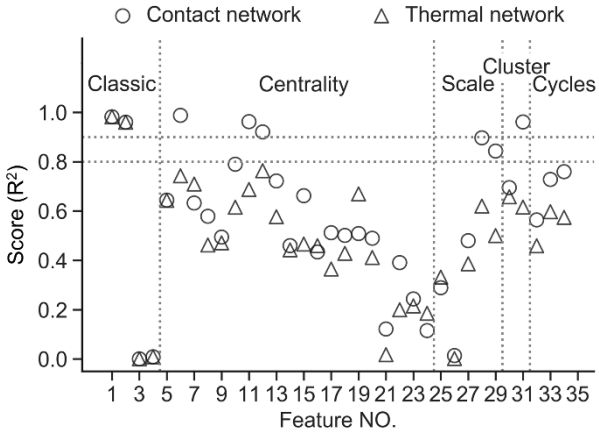

Fig. 19 Scores between network features and ETC in combined packings. The feature numbers are corresponding to Table 2.

$$\frac{\lambda_{eff}}{\lambda_{solid}} = -0.21([G^C]\kappa_w)^2 + 0.67[G^C]\kappa_w + 0.25 \quad (17)$$

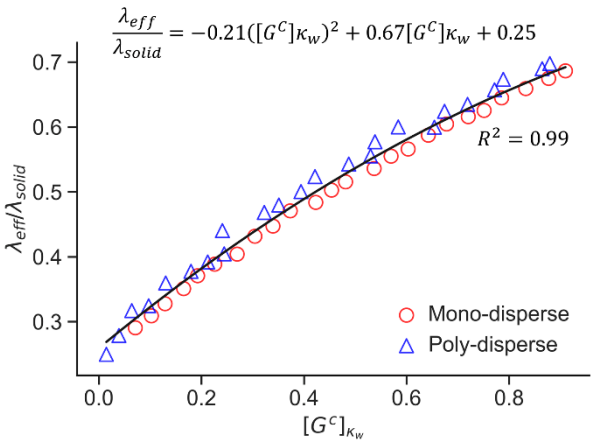

Fig. 20 The relationship between weighted degree from contact network and ETC.

Random forest scores are used to compute the score of the relationship between multi-network features and ETC as well as the relative importance of each feature. The score arising from testing thermal network features with random forest regression is around 0.94 which is higher than the score of an individual feature as shown in Fig. 19. The score of applying contact network features with random forest regression is calculated and around 0.98. The importance/relevance of each feature in a random forest regression is measured by Gini impurity [68] and shown in Fig. 21. The figure shows that weighted closeness centrality $[G^*]_{C_{nw1}}$ in either contact network or thermal network contributes the most when predicting ETC. The importance of $[G^*]_{C_{nw1}}$ hints again that a feature considering both particle connectivity and contact quality is crucial to predict ETC. Weighted degree $[G^*]_{\kappa_w}$ (Feature 6) is another important feature and it also measures both particle connectivity and contact quality. As for the rest of two relative important features, average weighted shortest path $[G^*]_{P_w}$ (Feature 28) is related to contact quality while local clustering coefficient $[G^*]_{LC}$ (Feature 31) is related to particle connectivity. Therefore, it is necessary to consider both contact quality and particle connectivity in a model for predicting ETC.

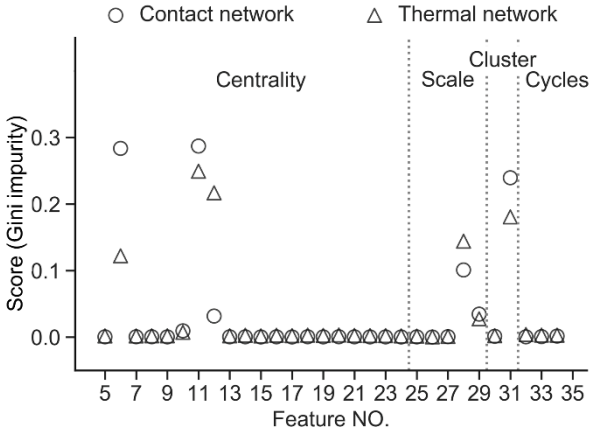

Fig. 21 Network feature importance in random forest regression models. (a) Contact network (b) Thermal network

Random forest regression shows the feasibility of predicting ETC using multi-network features. However, equations cannot be derived from the random forest algorithm because it is based on a branching series of Boolean tests. To clearly show the relationship between multiple thermal network features and ETC, $[G^T]_{C_{nw1}}$ (Feature 11) and $[G^*]_{LC}$ (Feature 31) are used to build a predictive Equation 18 from different types of features that show high scores (as depicted in Fig. 21):

$$\frac{\lambda_{eff}}{\lambda_{solid}} = -2879.4\left([G^T]_{C_{nw1}}\right)^2 + 61.6([G^T]_{LC})^2 + 133.5[G^T]_{C_{nw1}} - 46.6[G^C]\kappa_w + 7.78 \quad (18)$$

The resulting predictive equation has a high correlation coefficient R^2 of 0.96 as shown in Fig. 22, which indicates again the importance of particle connectivity and contact quality in heat transfer.

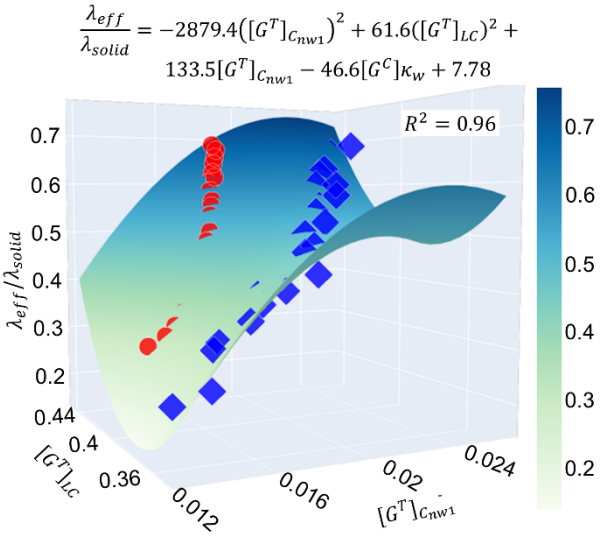

Fig. 22 The relationship between $[G^T]_{C_{nw1}}$ (weighted closeness centrality normalised by $[|V|(|V|-1)]/2$, $[G^T]_{LC}$ (local clustering coefficient) and ETC (https://wenbinfei.github.io/research_demos/5-sphere-network-features/).

4 Conclusion

A framework is proposed to select essential features (or new 'variables') which can be used to predict ETC. By computing the individual feature relevance to the ETC in mono-disperse and poly-disperse packings, we found individual network features can be alternatives to other classic or traditional parameters (such as porosity) when predicting ETC for mono-disperse and poly-disperse packings

respectively. Moreover, the correlations of features to ETC is higher in simpler mono-disperse packings than that in poly-disperse packings. By comparing the performance of individual contact network features and thermal network features on ETC, we found cluster and cycle features derived from the contact network to be more relevant than those arising from the thermal network. In contrast, centrality and scale features from the thermal network are more relevant than those from the contact network.

In order to analyse the general feature importance in a model that predicts the ETC in more extensive data set, the correlation of individual features with ETC was studied for combined mono-disperse and poly-disperse packings. Weighted degree $[G^c]_{kw}$, normalised weighted closeness centrality $[G^c]_{C_{nw1}}$and local clustering coefficient$[G^c]_{LC}$ from contact networks can still be used as individual features to predict ETC. Despite an individual thermal network feature rendering a relatively lower correlation to the ETC, random forest regression model with multiple thermal network features can achieve similar accuracy as that when using either an individual or multiple contact network features. The network feature involving both particle connectivity and contact quality always performs well in both small dataset size (mono-disperse packing or poly-disperse packing) and larger dataset size (combined mono-disperse and poly-disperse packings).

As computed tomography (CT) can be used to scan real granular materials and reconstruct their geometry [44], future work can expand on extracting the network features from these real materials and investigate the correlation with ETC.

Acknowledgements

We thank Min Zhang from the University of Nottingham Ningbo China for sharing the experience of generating multiple samples using PFC. This work is supported by the Melbourne Research Scholarship from The University of Melbourne.

References

[1] W.M. Rohsenow, J.P. Hartnett, E.N. Ganic, Handbook of heat transfer applications, New York, McGraw-Hill Book Co., 1985, 973 p. No individual items are abstracted in this volume., (1985).

[2] D.M. Scott, D.K. Das, V. Subbaihaannadurai, V.A. Kamath, A computational scheme for fluid flow and heat transfer analysis in porous media for recovery of oil and gas, Petroleum science and technology, 23 (2005) 843-862.

[3] W.B. Fei, Q. Li, X.C. Wei, R.R. Song, M. Jing, X.C. Li, Interaction analysis for CO2 geological storage and underground coal mining in Ordos Basin, China, Engineering geology, 196 (2015) 194-209.

[4] A.E. Bergles, J. Collier, J.M. Delhaye, G. Hewitt, F. Mayinger, Two-phase flow and heat transfer in the power and process industries, Hemisphere New York1981.

[5] W.H. Somerton, Thermal properties and temperature-related behavior of rock/fluid systems, Elsevier1992.

[6] H. KIVOHASHI, M. Deguchi, Derivation of a correlation formula for the effective thermal conductivity of geological porous materials by the three-phase geometric-mean model, High Temperatures. High Pressures, 30 (1998) 25-35.

[7] V. Odelevskii, Calculation of the generalized conductivity of heterogeneous systems, Zh. Tekh. Fiz, 21 (1951) 678-685.

[8] G. Dul'nev, Y.P. Zarichnyak, Thermal conductivity of mixtures and composite materials, Energiya, Leningrad, (1974).

[9] A. Mendel, Relation between thermal conductivity of rocks and structure of the pores, Russ J Geology Prospect, 1 (1997) 112-119.

[10] R. Krupiczka, Analysis of thermal conductivity in granular materials, International Chemical Engineering, 7 (1967) 122-+.

[11] Z. Abdulagatova, I. Abdulagatov, V. Emirov, Effect of temperature and pressure on the thermal conductivity of sandstone, International Journal of Rock Mechanics and Mining Sciences, 46 (2009) 1055-1071.

[12] J. Mo, H. Ban, Measurements and theoretical modeling of effective thermal conductivity of particle beds under compression in air and vacuum, Case studies in thermal engineering, 10 (2017) 423-433.

[13] T.S. Yun, J.C. Santamarina, Fundamental study of thermal conduction in dry soils, Granular matter, 10 (2008) 197.

[14] J. Sass, A.H. Lachenbruch, R.J. Munroe, Thermal conductivity of rocks from measurements on fragments and its application to heat-flow determinations, Journal of geophysical research, 76 (1971) 3391-3401.

[15] A.L. DeVera Jr, W. Strieder, Upper and lower bounds on the thermal conductivity of a random, two-phase material, The Journal of Physical Chemistry, 81 (1977) 1783-1790.

[16] A. Beck, An improved method of computing the thermal conductivity of fluid-filled sedimentary rocks, Geophysics, 41 (1976) 133-144.

[17] P. Yang, Y. Yu, L. Chen, W. Mao, Experimental determination and theoretical prediction of twin orientations in magnesium alloy AZ31, Scripta Materialia, 50 (2004) 1163-1168.

[18] C. Clauser, E. Huenges, Thermal conductivity of rocks and minerals, Rock physics & phase relations, 3 (1995) 105-126.

[19] F. Brigaud, G. Vasseur, Mineralogy, porosity and fluid control on thermal conductivity of sedimentary rocks, Geophysical Journal International, 98 (1989) 525-542.

[20] J.C. Maxwell, A treatise on electricity end magnetism, Clarendon Press, 1873.

[21] Y. Chiew, E. Glandt, The effect of structure on the conductivity of a dispersion, Journal of Colloid and Interface Science, 94 (1983) 90-104.

[22] E.E. Gonzo, Estimating correlations for the effective thermal conductivity of granular materials, Chemical Engineering Journal, 90 (2002) 299-302.

[23] J. Gan, Z. Zhou, A. Yu, Effect of particle shape and size on effective thermal conductivity of packed beds, Powder Technology, 311 (2017) 157-166.

[24] X. Huang, Q. Zhou, J. Liu, Y. Zhao, W. Zhou, D. Deng, 3D stochastic modeling, simulation and analysis of effective thermal conductivity in fibrous media, Powder technology, 320 (2017) 397-404.

[25] G. Wei, H. Zhang, X. An, B. Xiong, S. Jiang, CFD-DEM study on heat transfer characteristics and microstructure of the blast furnace raceway with ellipsoidal particles, Powder technology, 346 (2019) 350-362.
[26] G.K. Batchelor, R. O'brien, Thermal or electrical conduction through a granular material, Proc. R. Soc. Lond. A, 355 (1977) 313-333.
[27] J. Finney, Random packings and the structure of simple liquids. I. The geometry of random close packing, Proc. R. Soc. Lond. A, 319 (1970) 479-493.
[28] G. Cheng, A. Yu, P. Zulli, Evaluation of effective thermal conductivity from the structure of a packed bed, Chemical Engineering Science, 54 (1999) 4199-4209.
[29] W. Siu, S.-K. Lee, Effective conductivity computation of a packed bed using constriction resistance and contact angle effects, International journal of heat and mass transfer, 43 (2000) 3917-3924.
[30] I. Fatt, The network model of porous media, (1956).
[31] J.H. van der Linden, G.A. Narsilio, A. Tordesillas, Machine learning framework for analysis of transport through complex networks in porous, granular media: a focus on permeability, Physical Review E, 94 (2016) 022904.
[32] X. Huang, Y. He, W. Zhou, D. Deng, Y. Zhao, Pore network modeling of fibrous porous media of uniform and gradient porosity, Powder technology, 343 (2019) 350-361.
[33] M. Newman, Networks, Oxford university press2018.
[34] M.E. Newman, The structure and function of complex networks, SIAM review, 45 (2003) 167-256.
[35] S. Russell, D.M. Walker, A. Tordesillas, A characterization of the coupled evolution of grain fabric and pore space using complex networks: Pore connectivity and optimized flows in the presence of shear bands, Journal of the Mechanics and Physics of Solids, 88 (2016) 227-251.
[36] T.S. Yun, T.M. Evans, Three-dimensional random network model for thermal conductivity in particulate materials, Computers and Geotechnics, 37 (2010) 991-998.
[37] G. Cheng, J. Gan, D. Xu, A. Yu, Evaluation of effective thermal conductivity in random packed bed: Heat transfer through fluid voids and effect of packing structure, Powder Technology, (2019).
[38] P.D. Itasca, Particle Flow Code in 3 Dimensions, User's Guide, 2008.
[39] G.A. Narsilio, J. Kress, T.S. Yun, Characterisation of conduction phenomena in soils at the particle-scale: Finite element analyses in conjunction with synthetic 3D imaging, Computers and Geotechnics, 37 (2010) 828-836.
[40] P. Azadi, R. Farnood, N. Yan, FEM–DEM modeling of thermal conductivity of porous pigmented coatings, Computational Materials Science, 49 (2010) 392-399.
[41] T. Kanit, S. Forest, I. Galliet, V. Mounoury, D. Jeulin, Determination of the size of the representative volume element for random composites: statistical and numerical approach, International Journal of solids and structures, 40 (2003) 3647-3679.
[42] S. Ltd., Simpleware ScanIP, http://www.simpleware.com/software/scanip, Date of access, 15 (2015) 12.
[43] W. Fei, G.A. Narsilio, M.M. Disfani, Impact of three-dimensional sphericity and roundness on heat transfer in granular materials, Powder Technology, 355 (2019) 770-781.
[44] W. Fei, G.A. Narsilio, J.H. van der Linden, M.M. Disfani, Quantifying the impact of rigid interparticle structures on heat transfer in granular materials using networks, International Journal of Heat and Mass Transfer, 143 (2019) 118514.
[45] W.J. Bosl, J. Dvorkin, A. Nur, A study of porosity and permeability using a lattice Boltzmann simulation, Geophysical Research Letters, 25 (1998) 1475-1478.
[46] X. Garcia, L.T. Akanji, M.J. Blunt, S.K. Matthai, J.P. Latham, Numerical study of the effects of particle shape and polydispersity on permeability, Physical Review E, 80 (2009) 021304.
[47] C. AB, COMSOL multiphysics v5.0, http://www.comsol.com, (2015).
[48] H. Carslaw, J. Jaeger, Conduction of heat in solids: Oxford Science Publications, Oxford, England1959.
[49] J. Sundberg, P.-E. Back, L.O. Ericsson, J. Wrafter, Estimation of thermal conductivity and its spatial variability in igneous rocks from in situ density logging, International Journal of Rock Mechanics and Mining Sciences, 46 (2009) 1023-1028.

[50] R.E. Thalmann, Thermal conductivity of dry soils, University of Kansas, Mechanical Engineering, 1950.
[51] C. Argento, D. Bouvard, Thermal conductivity of granular media, Powders & grains, (1993) 129-134.
[52] L.C. Freeman, Centrality in social networks conceptual clarification, Social networks, 1 (1978) 215-239.
[53] L.C. Freeman, A set of measures of centrality based on betweenness, Sociometry, (1977) 35-41.
[54] A.N. Langville, C.D. Meyer, A survey of eigenvector methods for web information retrieval, SIAM review, 47 (2005) 135-161.
[55] D.M. Walker, A. Tordesillas, Topological evolution in dense granular materials: a complex networks perspective, International Journal of Solids and Structures, 47 (2010) 624-639.
[56] R. Arévalo, I. Zuriguel, D. Maza, Topology of the force network in the jamming transition of an isotropically compressed granular packing, Physical Review E, 81 (2010) 041302.
[57] A. Tordesillas, D.M. Walker, Q. Lin, Force cycles and force chains, Physical Review E, 81 (2010) 011302.
[58] R. Arevalo, I. Zuriguel, D. Maza, Topological properties of the contact network of granular materials, International Journal of Bifurcation and Chaos, 19 (2009) 695-702.
[59] D.S. Bassett, E.T. Owens, K.E. Daniels, M.A. Porter, Influence of network topology on sound propagation in granular materials, Physical Review E, 86 (2012) 041306.
[60] A. Tordesillas, Q. Lin, J. Zhang, R. Behringer, J. Shi, Structural stability and jamming of self-organized cluster conformations in dense granular materials, Journal of the Mechanics and Physics of Solids, 59 (2011) 265-296.
[61] D.J. Watts, S.H. Strogatz, Collective dynamics of 'small-world'networks, nature, 393 (1998) 440.
[62] F. Santosa, W.W. Symes, Linear inversion of band-limited reflection seismograms, SIAM Journal on Scientific and Statistical Computing, 7 (1986) 1307-1330.
[63] F. Pedregosa, G. Varoquaux, A. Gramfort, V. Michel, B. Thirion, O. Grisel, M. Blondel, P. Prettenhofer, R. Weiss, V. Dubourg, Scikit-learn: Machine learning in Python, Journal of machine learning research, 12 (2011) 2825-2830.
[64] T.K. Ho, Random decision forests, Document analysis and recognition, 1995., proceedings of the third international conference on, IEEE, 1995, pp. 278-282.
[65] I. Barandiaran, The random subspace method for constructing decision forests, IEEE transactions on pattern analysis and machine intelligence, 20 (1998).
[66] B. Kamiński, M. Jakubczyk, P. Szufel, A framework for sensitivity analysis of decision trees, Central European journal of operations research, 26 (2018) 135-159.
[67] M. Stone, Cross-validatory choice and assessment of statistical predictions, Journal of the royal statistical society. Series B (Methodological), (1974) 111-147.
[68] P. Breheny, Classification and regression trees, (1984).
[69] J. Koh, A. Fortini, Thermal conductivity and electrical resistivity of porous material, (1971).
[70] J. Agapiou, M. DeVries, An experimental determination of the thermal conductivity of a 304L stainless steel powder metallurgy material, Journal of Heat Transfer, 111 (1989) 281-286.
[71] S. Torquato, I.C. Kim, D. Cule, Effective conductivity, dielectric constant, and diffusion coefficient of digitized composite media via first-passage-time equations, Journal of Applied Physics, 85 (1999) 1560-1571.
[72] U. Ayachit, The paraview guide: a parallel visualization application, Kitware, Inc.2015.
[73] U. El Shamy, O. De Leon, R. Wells, Discrete element method study on effect of shear-induced anisotropy on thermal conductivity of granular soils, International Journal of Geomechanics, 13 (2013) 57-64.
[74] Y. Hu, J. Wang, J. Yang, I. Mudawar, Q. Wang, Experimental study of forced convective heat transfer in grille-particle composite packed beds, International Journal of Heat and Mass Transfer, 129 (2019) 103-112.
[75] R. Askari, S.H. Hejazi, M. Sahimi, Thermal Conduction in Deforming Isotropic and Anisotropic Granular Porous Media with Rough Grain Surface, Transport in Porous Media, 124 (2018) 221-236.
[76] B. Aduda, Effective thermal conductivity of loose particulate systems, Journal of materials science, 31 (1996) 6441-6448.

845 [77] M. Gangadhara Rao, D. Singh, A generalized relationship to estimate thermal resistivity of soils,
846 Canadian Geotechnical Journal, 36 (1999) 767-773.
847 [78] J. Côté, J.-M. Konrad, Thermal conductivity of base-course materials, Canadian Geotechnical
848 Journal, 42 (2005) 61-78.
849 [79] L. Fletcher, Recent developments in contact conductance heat transfer, Journal of Heat Transfer,
850 110 (1988) 1059-1070.
851 [80] Y. Asakuma, M. Asada, Y. Kanazawa, T. Yamamoto, Thermal analysis with contact resistance of
852 packed bed by a homogenization method, Powder technology, 291 (2016) 46-51.
853
854

Appendix

Appendix 1 Contact network feature importance

Type	NO.	Notation	Mono-disperse packings		Poly-disperse packings	
			Score	Model	Score	Model
Classic	1	n	0.9995	Quadratic polynomial	0.9979	Linear
	2	γ	0.9988	Exponential	0.9951	Exponential
	3	C_u	0.0000	Quadratic polynomial	0.0289	Quadratic polynomial
	4	C_c	0.0000	Quadratic polynomial	0.0012	Linear
Centrality	5	$[G^c]_{\kappa}$	0.9986	Power	0.9871	Quadratic polynomial
	6	$[G^c]_{\kappa_w}$	0.9990	Quadratic polynomial	0.9949	Cubic Polynomial
	7	$[\mathrm{G^c}]_{\mathrm{C}}$	0.9945	Logarithmic	0.9345	Logarithmic
	8	$[\mathrm{G^c}]_{\mathrm{C_{n1}}}$	0.2251	Linear	0.9131	Logarithmic
	9	$[G^c]_{C_{n2}}$	0.9971	Linear	0.9677	Logarithmic
	10	$[G^c]_{C_w}$	0.9982	Exponential	0.9339	Linear
	11	$[G^c]_{C_{nw1}}$	0.9992	Linear	0.9652	Quadratic polynomial
	12	$[G^c]_{C_{nw2}}$	0.9989	Quadratic polynomial	0.9777	Quadratic polynomial
	13	$[G^c]_{B^{node}}$	0.9939	Logarithmic	0.9259	Logarithmic
	14	$[G^c]_{B_n^{node}}$	0.9972	Quadratic polynomial	0.9707	Quadratic polynomial
	15	$[G^c]_{B_w^{node}}$	0.9864	Quadratic polynomial	0.9039	Logarithmic
	16	$[G^c]_{B_{nw}^{node}}$	0.9965	Exponential	0.9665	Exponential
	17	$[G^c]_{B^{edge}}$	0.4738	Power	0.7695	Exponential
	18	$[G^c]_{B_n^{edge}}$	0.9983	Quadratic polynomial	0.9811	Cubic Polynomial
	19	$[G^c]_{B_w^{edge}}$	0.3120	Exponential	0.8253	Exponential
	20	$[G^c]_{B_{nw}^{edge}}$	0.9983	Cubic Polynomial	0.9803	Cubic Polynomial
	21	$[G^c]_{B_w^{edge^{tp}}}$	0.2567	Power	0.4748	Logarithmic
	22	$[G^c]_{B_{nw}^{edge^{tp}}}$	0.9679	Exponential	0.9269	Quadratic polynomial
	23	$[G^c]_E$	0.4256	Exponential	0.2324	Exponential
	24	$[G^c]_{E_w}$	0.9283	Quadratic polynomial	0.3574	Power
Network scale	25	G_ρ^c	0.6126	Exponential	0.3729	Power
	26	G_D^c	0.0006	Logarithmic	0.3147	Exponential
	27	$G_{D_n}^c$	0.8955	Logarithmic	0.9323	Power
	28	$[G^c]_{P_w}$	0.9731	Power	0.9010	Power
	29	$[G^c]_{P_w}^{\mathrm{tp}}$	0.9727	Power	0.8438	Power
Clustering	30	$G^c{}_{GC}$	0.9942	Quadratic polynomial	0.9840	Exponential
	31	$[G^c]_{LC}$	0.9880	Quadratic polynomial	0.9801	Quadratic polynomial
Cycles	32	G_{3C}^c	0.9985	Quadratic polynomial	0.9869	Quadratic polynomial
	33	$[G^c]_{3C^{node}}$	0.9978	Quadratic polynomial	0.9898	Quadratic polynomial
	34	$[G^c]_{3C^{\mathrm{edge}}}$	0.9968	Quadratic polynomial	0.9893	Linear

Appendix 2 Thermal network feature importance

Type	NO.	Notation	Mono-disperse packings		Poly-disperse packings	
			Score	Model	Score	Model
Classic	1	n	0.9995	Quadratic polynomial	0.9979	Linear
	2	γ	0.9988	Exponential	0.9951	Exponential
	3	C_u	0.0000	Quadratic polynomial	0.0289	Quadratic polynomial
	4	C_c	0.0000	Quadratic polynomial	0.0009	Logarithmic
Centrality	5	$[G^T]_{\kappa}$	0.9939	Linear	0.9363	Logarithmic
	6	$[G^T]_{\kappa w}$	0.9992	Quadratic polynomial	0.9905	Quadratic polynomial
	7	$[\mathrm{G^T}]_{\mathrm{C}}$	0.9957	Logarithmic	0.8682	Logarithmic
	8	$[\mathrm{G^T}]_{\mathrm{C_{n1}}}$	0.9525	Logarithmic	0.1295	Quadratic polynomial
	9	$[G^T]_{C_{n2}}$	0.9958	Logarithmic	0.9010	Cubic Polynomial
	10	$[G^T]_{C_w}$	0.3390	Linear	0.9169	Exponential
	11	$[G^T]_{C_{nw1}}$	0.9967	Cubic Polynomial	0.9929	Exponential
	12	$[G^T]_{C_{nw2}}$	0.9984	Quadratic polynomial	0.9854	Quadratic polynomial
	13	$[G^T]_{B^{node}}$	0.9953	Logarithmic	0.8617	Logarithmic
	14	$[G^T]_{B_n^{node}}$	0.9955	Logarithmic	0.9013	Cubic Polynomial
	15	$[G^T]_{B_w^{node}}$	0.9942	Logarithmic	0.6195	Linear
	16	$[G^T]_{B_{nw}^{node}}$	0.9972	Quadratic polynomial	0.9506	Cubic Polynomial
	17	$[G^T]_{B^{edge}}$	0.9825	Logarithmic	0.0373	Logarithmic
	18	$[G^T]_{B_n^{edge}}$	0.9958	Logarithmic	0.9261	Cubic Polynomial
	19	$[G^T]_{B_w^{edge}}$	0.9792	Logarithmic	0.5534	Exponential
	20	$[G^T]_{B_{nw}^{edge}}$	0.9970	Quadratic polynomial	0.9459	Logarithmic
	21	$[G^T]_{B_w^{edge^{tp}}}$	0.6845	Cubic Polynomial	0.0747	Exponential
	22	$[G^T]_{B_{nw}^{edge^{tp}}}$	0.9289	Logarithmic	0.8540	Cubic Polynomial
	23	$[G^T]_E$	0.8378	Logarithmic	0.1361	Linear
	24	$[G^T]_{E_w}$	0.3541	Cubic Polynomial	0.3570	Logarithmic
Network scale	25	G_ρ^T	0.9856	Linear	0.1210	Logarithmic
	26	G_D^T	0.0450	Logarithmic	0.0002	Logarithmic
	27	$G_{D_n}^T$	0.9335	Exponential	0.6939	Linear
	28	$[G^T]_{P_w}$	0.9958	Cubic Polynomial	0.9839	Power
	29	$[G^T]_{P_w^{\mathrm{tp}}}$	0.9932	Cubic Polynomial	0.9665	Cubic Polynomial
Clustering	30	$G^T{}_{GC}$	0.9862	Quadratic polynomial	0.9248	Logarithmic
	31	$[G^T]_{LC}$	0.9785	Quadratic polynomial	0.9218	Logarithmic
Cycles	32	G_{3C}^T	0.9955	Quadratic polynomial	0.9321	Quadratic polynomial
	33	$[G^T]_{3C^{node}}$	0.9925	Quadratic polynomial	0.9309	Logarithmic
	34	$[G^T]_{3C^{\mathrm{edge}}}$	0.9913	Linear	0.9260	Logarithmic

Appendix 3 Feature importance in combined samples

Type	NO.	Notation	Contact network		Thermal network	
			Score	Model	Score	Model
Classic	1	n	0.9819	Linear	0.9819	Linear
	2	γ	0.9599	Exponential	0.9599	Exponential
	3	C_u	0.0004	Logarithmic	0.0004	Logarithmic
	4	C_c	0.0088	Quadratic polynomial	0.0088	Quadratic polynomial
Centrality	5	$[G^*]_{\kappa}$	0.6441	Logarithmic	0.6428	Cubic Polynomial
	6	$[G^*]_{\kappa_w}$	0.9877	Quadratic polynomial	0.7427	Logarithmic
	7	$[\mathrm{G}^*]_{\mathrm{C}}$	0.6323	Cubic Polynomial	0.7092	Cubic Polynomial
	8	$[\mathrm{G}^*]_{\mathrm{C_{n1}}}$	0.5785	Cubic Polynomial	0.4619	Cubic Polynomial
	9	$[G^*]_{C_{n2}}$	0.4941	Cubic Polynomial	0.4708	Cubic Polynomial
	10	$[G^*]_{C_w}$	0.7895	Power	0.6152	Cubic Polynomial
	11	$[G^*]_{C_{nw1}}$	0.9622	Quadratic polynomial	0.6870	Quadratic polynomial
	12	$[G^*]_{C_{nw2}}$	0.9205	Cubic Polynomial	0.7631	Logarithmic
	13	$[G^*]_{B^{node}}$	0.7217	Cubic Polynomial	0.5765	Cubic Polynomial
	14	$[G^*]_{B_n^{node}}$	0.4594	Linear	0.4422	Cubic Polynomial
	15	$[G^*]_{B_w^{node}}$	0.6619	Cubic Polynomial	0.4658	Cubic Polynomial
	16	$[G^*]_{B_{nw}^{node}}$	0.4339	Linear	0.4592	Linear
	17	$[G^*]_{B^{edge}}$	0.5118	Cubic Polynomial	0.3646	Cubic Polynomial
	18	$[G^*]_{B_n^{edge}}$	0.5009	Linear	0.4282	Cubic Polynomial
	19	$[G^*]_{B_w^{edge}}$	0.5084	Cubic Polynomial	0.6692	Quadratic polynomial
	20	$[G^*]_{B_{nw}^{edge}}$	0.4893	Linear	0.4113	Cubic Polynomial
	21	$[G^*]_{B_w^{edge^{tp}}}$	0.1215	Logarithmic	0.0175	Logarithmic
	22	$[G^*]_{B_{nw}^{edge^{tp}}}$	0.3906	Linear	0.1994	Linear
	23	$[G^*]_E$	0.2434	Cubic Polynomial	0.2151	Logarithmic
	24	$[G^*]_{E_w}$	0.1151	Linear	0.1851	Cubic Polynomial
Network scale	25	G_ρ^*	0.2888	Cubic Polynomial	0.3318	Cubic Polynomial
	26	G_D^*	0.0138	Logarithmic	0.0016	Logarithmic
	27	$G_{D_n}^*$	0.4796	Linear	0.3857	Linear
	28	$[G^*]_{P_w}$	0.8965	Power	0.6198	Quadratic polynomial
	29	$[G^*]_{P_w^{tp}}$	0.8429	Power	0.5002	Cubic Polynomial
Clustering	30	$G^*{}_{GC}$	0.6947	Logarithmic	0.6574	Cubic Polynomial
	31	$[G^*]_{LC}$	0.9609	Quadratic polynomial	0.6156	Linear
Cycles	32	G_{3C}^*	0.5638	Logarithmic	0.4588	Cubic Polynomial
	33	$[G^*]_{3C^{node}}$	0.7279	Logarithmic	0.5971	Cubic Polynomial
	34	$[G^*]_{3C^{\mathrm{edge}}}$	0.7593	Logarithmic	0.5740	Cubic Polynomial

List of Figures

Fig. 16. ETC monotonically and smoothly decreases with the increasing average weighted shortest path GTPw calculated from a thermal network.

Fig. 17. The relationship between ETC and (a) Global clustering coefficient and (b) 3-cycle. Points in the figure represent the data used to train models while lines represent the predicted values from selected models.

Fig. 18. A heatmap shows the score of correlation between a different pair of features in poly-disperse packings. Feature 0 is the ETC and other feature numbers refer to Table 2.

Fig. 19. Scores between network features and ETC in combined packings. The feature numbers are corresponding to Table 2.

Fig. 20. The relationship between weighted degree from contact network and ETC.s

Fig. 21. Network feature importance in random forest regression models. (a) Contact network (b) Thermal network

Fig. 22. The relationship between $[G^T]_{c_{nw1}}$(weighted closeness centrality normalised by $[|\mathrm{V}|(|\mathrm{V}|-1)]/2$, $[\mathrm{G^T}]_{\mathrm{LC}}$ (local clustering coefficient) and ETC (https://wenbinfei.github.io/research_demos/5-sphere-network-features/).

List of Tables